Journal of Nuclear Materials 404 (2010) 128–137

Contents lists available at ScienceDirect

Journal of Nuclear Materials

journal homepage: www.elsevier.com/locate/jnucmat

UO_2/Zry-4 chemical interaction layers for intact and leak PWR fuel rods

Kyu-Tae Kim *

Dongguk University, College of Energy & Environment, 707 Seokjang-Dong, Gyeongju, Gyeongbuk 780-714, Republic of Korea

ARTICLE INFO

Article history:
Received 11 October 2009
Accepted 5 July 2010

ABSTRACT

In this study, the UO_2 pellet–Zry-4 cladding interfaces of intact and leak PWR fuel rods were examined with the help of an optical microscope and a scanning electron microscope to investigate typical chemical interaction layers formed at the pellet–cladding interface during the normal reactor operations. The two intact and two leak fuel rods with the burnup of between 35,000 and 53,000 MWD/MTU were selected to evaluate the effects of gap–gas compositions and fuel burnup on the chemical interaction layer formation. Based on the optical and scanning electron micrographs, it is found that the intact fuel rod generates apparently one interaction layer of $(U,Zr)O_{2-x}$ at the interface, whereas the leak fuel rod generates apparently two interaction layers of ZrO_{2-x} and $(U,Zr)O_{2-x}$. These interaction layers for the intact and leak fuel rods were predicted by several diffusion paths drawn on a U–Zr–O ternary phase diagram. The variations of chemical element compositions around the interface of one intact rod were generated by an electron probe micro-analyzer to confirm the interaction layers at the pellet–cladding interface. The interaction layer growth rates of the ZrO_{2-x} and $(U,Zr)O_{2-x}$ phases were estimated, using the layer thicknesses and the reaction times.

1. Introduction

Zircaloy and UO_2 are known to be thermodynamically unstable with respect to each other, even under normal nuclear reactor operating conditions, resulting in various chemical interaction layers. In general, the reaction rate increases with the increase of temperature and Zircaloy can react with solid UO_2 as either a solid or a liquid. A great many data for chemical interactions between liquid Zircaloy and solid UO_2 have been generated by various out-of-pile experiments [1–6] that have been utilized in simulating the reactor core meltdown phenomena under degraded reactor core accidents. In addition, a few data for chemical interactions between solid Zircaloy and solid UO_2 have been generated by various out-of-pile experiments in the temperature range of between 1000 and 1700 °C [7]. The out-of-pile experiments with the solid Zircaloy and solid UO_2 specimens [7] indicate that three chemical interaction layers are formed at the Zircaloy and UO_2 interface, which are [α-Zr(O) + (U,Zr)], [U,Zr] and α-Zr(O). It was reported that the interfacial energies of Zircaloy and UO_2 are such that three-layer sequence is energetically more stable than is two-layer one, and so the three-layer sequence is the one that is experimentally observed. In addition, each layer was found to follow the parabolic rate laws. It was also reported that the reaction rate is low enough at normal reactor operating temperatures to make the reaction negligible. In the normal reactor operating temperature of around 400 °C, however, the formation of the pellet–cladding interaction layers with specific chemical, physical and mechanical properties is of importance regarding the evolution of thermal conductivity as well as in the context of the pellet–cladding mechanical interaction. It is also important in the framework of long-term storage of spent fuel where the phases formed at the pellet–cladding interface are considered to be the first to be leached in the case of the cladding failure. Under normal reactor operating conditions, the UO_2 pellet–Zircaloy cladding gap in the fuel rods of LWRs tends to close up due to pellet swelling and cladding creep-down, and eventually a bonding layer may be formed between the pellet and the cladding usually at high burnup. According to in-reactor operating experiences of high burnup fuel rods, the chemical interaction layers between the pellet–cladding interfaces were observed [8–10] but the formation conditions of complex layers and the chemical compositions are much less documented. In this study, the pellet–cladding interfaces of the intact and leak PWR fuel rods with a relatively high burnup were examined with the help of an optical microscope, a scanning electron microscope and an electron probe micro-analyzer in order to investigate the characteristics of the chemical interaction layers formed at the interfaces during the normal reactor operations. Then, the chemical interaction layers observed at the interfaces were predicted with the help of a U–Zr–O ternary phase diagram [11,12]. In addition, the difference in the chemical interaction layers between the intact fuel rods and the leak ones was explained, considering the difference in the gap–gas compositions for the intact and leak fuel rods. The interaction layers observed in this study were also

* Tel.: +82 11 9805 1447; fax: +82 54 770 2282.
E-mail address: ktkim@dongguk.ac.kr

0022-3115/$ - see front matter © 2010 Elsevier B.V. All rights reserved.
doi:10.1016/j.jnucmat.2010.07.013

compared with some out-of-pile interaction layers at the temperatures of 1000–1700 °C reported in [7].

2. Experimental

2.1. Fuel samples

The pellet–cladding bonding and the formation of multi chemical interaction layers are usually observed for high burnup and/or high duty fuel. To investigate the interaction layers formed at the pellet–cladding interface, four PWR fuel rods with a relatively high burnup and high duty were selected from the fuel assemblies that had been irradiated in the two-loop and three-loop nuclear power plants operating in Korea. The fuel rods are composed of two intact fuel rods and two leak rods. The burnup of the fuel rods is in the range of between 35,000 and 53,000 MWD/MTU. The root cause of the leak rod for the two-loop plant is grid-to-rod fretting wear-induced failure that occurred at about 100 days from the startup of the twice-burned cycle corresponding to the burnup of about 22,000 MWD/MTU, whereas that for the three-loop plant is excessive cladding oxidation-induced failure combined with the pellet–clad interaction that occurred at about 250 days from the startup of the thrice-burned cycle corresponding to 40,000 MWD/MTU. For simplification, the fuel rods A, B, C and D denote the intact fuel rod of 53,000 MWD/MTU for the three-loop plant, that of 35,000 MWD/MTU for the two-loop plant, the leak fuel rod of 48,000 MWD/MTU for the three-loop plant and that of 35,000 MWD/MTU for the two-loop plant. The operating conditions of the two-loop and three-loop nuclear power plants operating in Korea are summarized in Table 1. In addition, the fuel rods considered in this study are given in Table 2.

2.2. Sample preparation and examination

Hot cell examinations were performed by two steps, i.e., non-destructive and destructive tests. The non-destructive tests are composed of visual examination of fuel rod surface, eddy current test, gamma scanning and rod pressure measurements. The fuel rods selected in this study were cut in an axial direction and in a radial one at specified axial positions. The specimens prepared by cutting were imbedded in epoxy resin and polished with diamond grinding discs of successively finer grain size, finishing on cloth with diamond paste. Because of radiation shielding problem, the UO_2 pellet was eliminated from the EPMA specimens that were cut with 2 mm in length. Before mounting the specimens in the electron microscope, the specimens were coated with carbon to prevent charging. To find out chemical interaction layers formed at the pellet–cladding interface, optical microscopy was performed on a shielded optical microscope equipped with a digital image acquisition system. Scanning electron microscopy was also performed on a shielded Phillips XL30 microscope to compensate optical microscopy for examining interaction layers. The electron probe micro-analyzer (EPMA) equipped with two wavelength dispersive spectroscopy (WDS) was used to generate chemical compositions of interaction layers.

Table 1
Operation conditions of two- and three-loop plants.

Parameters	Two-loop plant	Three-loop plant
Reactor power (MWe)	650	950
Linear power rating (kW/m)	17.61	17.83
Cycle length (months)	15	18
Fuel assembly type	16 × 16	17 × 17
Fuel rod diameter (mm)	9.50	9.50
Initial pellet-to-clad gap (mm)	0.082	0.082

3. Results and discussion

The optical micrographs of the intact fuel rod A are shown in Figs. 1 and 2. Fig. 1 shows grey colored ZrO_2, α-Zr(O) with typical radial hydride distribution, grey $(U,Zr)O_{2-x}$ and UO_2 pellet when moving from the cladding outer surface to the pellet side. The chemical interaction layer of grey $(U,Zr)O_{2-x}$ will be explained later with the use of the U–Zr–O ternary phase diagram [11,12]. As shown in Fig. 3 [13], it should be noted that an oxidized Zr metal exists as HCP-phased α-Zr(O) containing oxygen up to 30 mol percent in the normal reactor operation temperature range of between 400–500 °C. Fig. 2 shows one chemical interaction layer, $(U,Zr)O_{2-x}$, can be clearly found at the pellet–clad interfaces except at the lower axial position having no pellet–cladding hard contact. The largest waterside ZrO_2 oxide layer thickness for the intact rod A is in the range of 130 μm and the maximum thickness of the $(U,Zr)O_{2-x}$ interaction layer is about 12 μm at the mid-axial position with the hard pellet–cladding contact. Similar images of the fuel rod A were generated with scanning electron microscopy, as shown in Fig. 4. These images indicate two different colored α-$Zr(O)_I$ and α-$Zr(O)_{II}$ layers in the cladding, $(U,Zr)O_{2-x}$ interaction layer and the UO_2 pellet from the left to the right. The α-$Zr(O)_I$ and $Zr(O)_{II}$ layers may be oxygen-deficient and oxygen-saturated α-Zr(O), respectively, which will be explained later with the use of the U–Zr–O ternary phase diagram [11,12]. It is noteworthy that the non-porous microstructures of the $(U,Zr)O_{2-x}$ interaction layer and the thin UO_2 layer formed adjacent to the $(U,Zr)O_{2-x}$ layer are quite different from the porous original UO_2 pellet. In addition, the bonding configurations between the $(U,Zr)O_{2-x}$ and the UO_2 pellet/the Zr cladding are very strong as witnessed by the fact that every part of the $(U,Zr)O_{2-x}$ layer is found to adhere to the pellet and the cladding. It should be noted that the interface between the interaction layer and the pellet is relatively more irregular than that between the interaction layer and the cladding. This irregularity of the interface between the $(U,Zr)O_{2-x}$ layer and the UO_2 pellet may be explained by preferential diffusion of chemical elements along the UO_2 pellet grain boundaries since grain boundary diffusion is faster than trans-granular diffusion. With the use of the electron probe micro-analyzer (EPMA), on the other hand, the chemical composition variation of U, Zr and O at the chemical interaction layer was produced, as shown in Fig. 5. From this figure, it can be seen that the interaction layer is a mixture of U, Zr and O, indicating that Zr is diffusing into the UO_2 pellet side,

Table 2
Chemical interaction layer thicknesses and growth rates.

Plant types	Rod types	Rod conditions	Chemical interaction layers	Layer thicknesses (X)	Interaction times (t)	Growth rate (X^2/t)
Three-loop plant	Rod A	Intact (53,000 MWD/MTU)	$(U,Zr)O_{2-x}$	12 μm	416 days	4.0×10^{-14} cm^2/s
Two-loop plant	Rod B	Intact (35,000 MWD/MTU)	$(U,Zr)O_{2-x}$	9 μm	260 days	3.6×10^{-14} cm^2/s
Three-loop plant	Rod C	Failed (48,000 MWD/MTU)	ZrO_{2-x}	15 μm	166 days	1.6×10^{-13} cm^2/s
			$(U,Zr)O_{2-x}$	12 μm	416 days	4.0×10^{-14} cm^2/s
Two-loop plant	Rod D	Failed (35,000 MWD/MTU)	ZrO_{2-x}	15 μm	280 days	9.3×10^{-14} cm^2/s
			$(U,Zr)O_{2-x}$	6 μm	260 days	1.6×10^{-14} cm^2/s

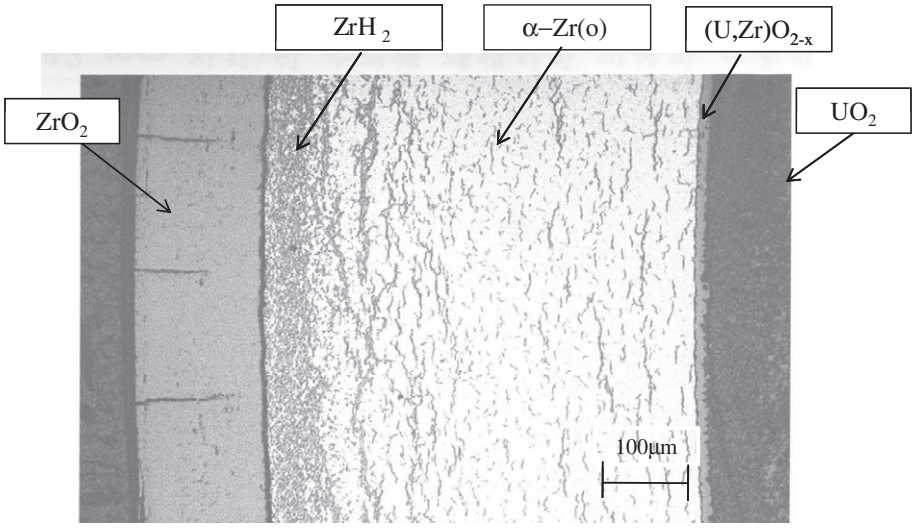

Fig. 1. An optical micrograph of intact fuel rod A.

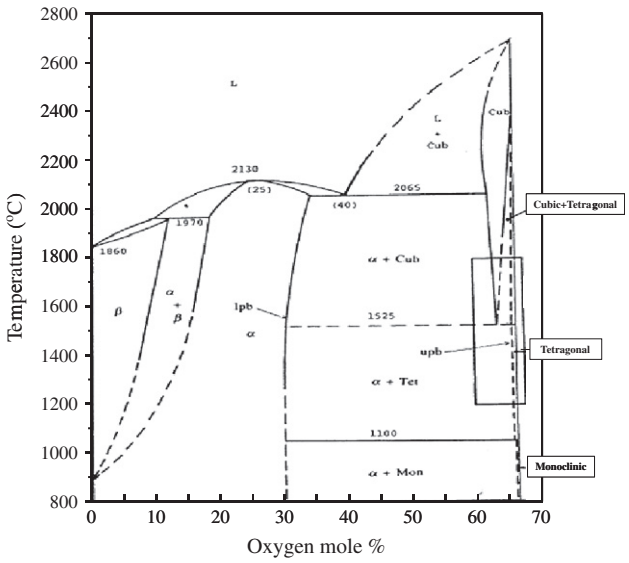

Fig. 2. A Zr–O phase diagram [13].

while U and O into the Zr cladding side. The oxygen content in the Zr metal (see region A in Fig. 5) is increasing in moving to the cladding–pellet interface to finally form oxygen-saturated α-Zr(O) at the interface of the Zr metal phase and the $(U,Zr)O_{2-x}$ phase. The oxygen content of the $(U,Zr)O_{2-x}$ phase (see region B in Fig. 5) is about 62 a/o, while the U and Zr contents vary sharply across the $(U,Zr)O_{2-x}$ phase. On the other hand, Fig. 6 shows chemical composition variations of some fission products such as Cs, Nd, Mo and Ru around the chemical interaction layers at the pellet–cladding interface that were analyzed by the EPMA. From this figure, one can say that the diffusion of Ru into the interaction layer is negligible but Cs moves faster than U and is found even in the cladding region. On the other hand, the optical micrographs of the intact fuel rod B are shown in Fig. 7. Just like the intact fuel rod A, one chemical interaction layer can be clearly found at the interface. However, the interaction layer is not visible at all radial locations at mid-axial position, but it covers roughly 50% of the pellet–cladding interface. The largest waterside ZrO_2 oxide layer thickness for the fuel rod B is in the range of 30 μm, while the maximum chemical interaction layer thickness is about 9 μm at the mid-axial position with the hard pellet–cladding contact.

On the other hand, the optical micrographs of the leak fuel rod C are shown in Fig. 8. From this figure, it can be seen that two chemical interaction layers of ZrO_2 and $(U,Zr)O_{2-x}$ rather than one interaction layer of $(U,Zr)O_{2-x}$ can be clearly found at the interface. From Fig. 8, it can be seen that the two interaction layers have quite different microstructures with respect to porosity and interface irregularity. The $(U,Zr)O_{2-x}$ phase has a lot of big voids in the matrix and an irregular interface between the $(U,Zr)O_{2-x}$ interaction layer and the UO_2 pellet, while the ZrO_2 phase has almost no void in the matrix and nearly a flat interface between the ZrO_2 interaction layer and the cladding metal region. It should be noted that the $(U,Zr)O_{2-x}$ layer for the intact fuel rods A and B does not contain any pore at all. Therefore, it can be said that the porous microstructure of $(U,Zr)O_{2-x}$ layer for the leak rod may be caused by the reaction of steam in the gap with the $(U,Zr)O_{2-x}$ phase. The largest waterside ZrO_2 oxide layer thickness for the leak rod C is in the range of 180 μm, while the maximum ZrO_2 and $(U,Zr)O_{2-x}$ layer thicknesses at the pellet–cladding contact surfaces for the leak rod C are about 15 and 12 μm, respectively, at the mid-axial position with the hard contact. On the other hand, the optical micrographs of the leak fuel rod D are shown in Fig. 9. Just like the leak fuel rod C, the ZrO_2 and $(U,Zr)O_{2-x}$ layers are clearly found at the pellet–cladding hard contact interfaces of the mid-axial position, while the ZrO_2 layer only is found on the cladding inner surface at the lower axial position since there is no hard pellet–cladding contact. However, the two interaction layers are visible at all radial locations at the mid-axial position, indicating that the hard contact formed at all radial locations. It should be noted that the $(U,Zr)O_{2-x}$ layer for the leak rod D is much less porous than that for the leak rod C. This may be explained by the fact that the cladding breach occurred before the pellet–clad hard contact of the leak rod D and thus the UO_2 pellet started to react with the already-formed ZrO_2 layer on the cladding inner surface to form the less porous $(U,Zr)O_{2-x}$. The estimation of the onset times for cladding breach and the pellet–clad hard contact will be discussed later in this chapter. The largest waterside ZrO_2 oxide layer thickness for the leak rod D is about 30 μm and the pellet side ZrO_2 oxide layer thickness is about 5 μm at the lower axial position having no hard contact. However, the maximum ZrO_2 and $(U,Zr)O_{2-x}$ layer thicknesses for the leak rod D are about 15 and 6 μm, respectively, at the mid-axial position having the hard contact.

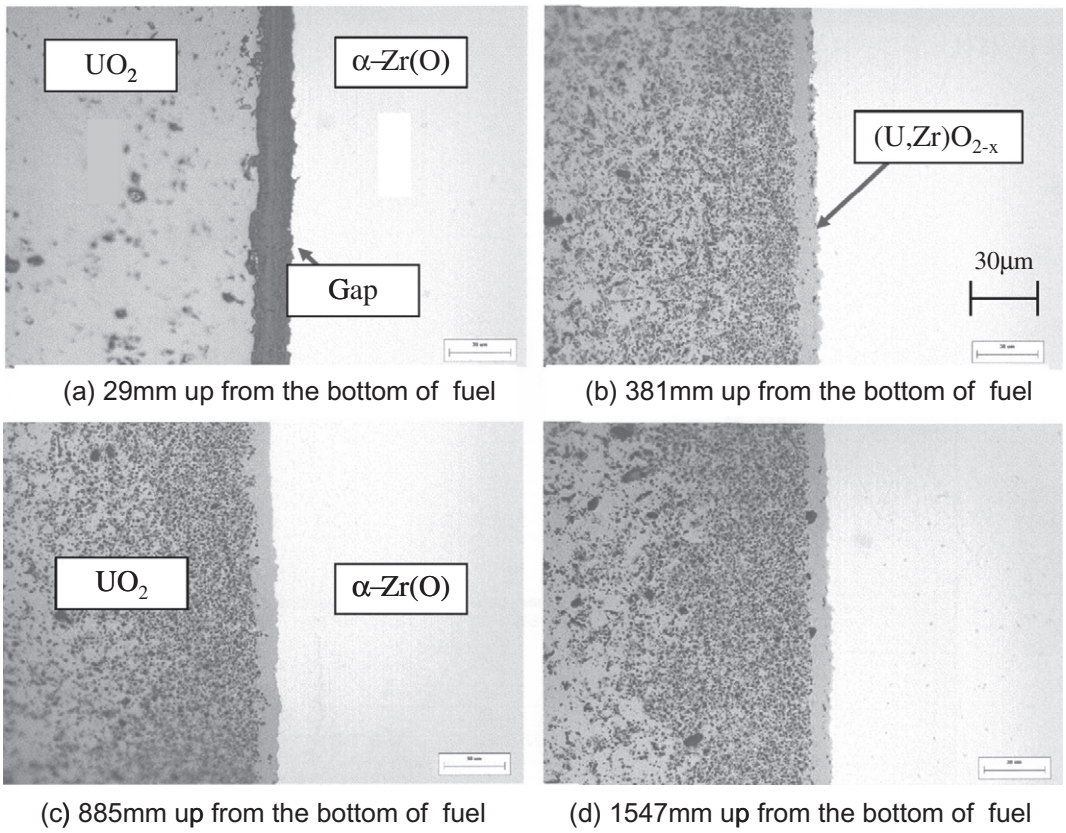

Fig. 3. Optical micrographs of intact fuel rod A.

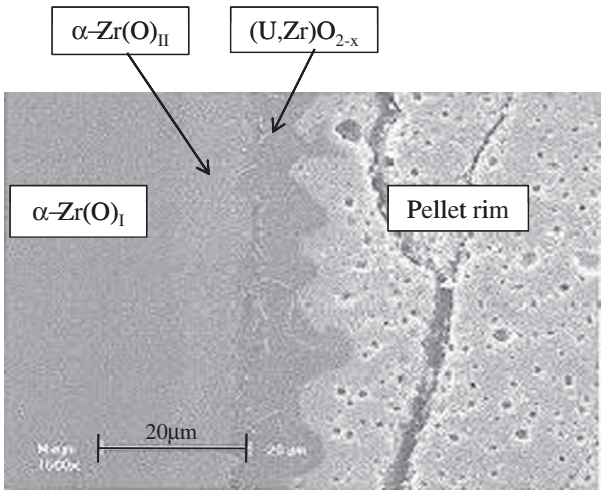

Fig. 4. A scanning electron micrograph of intact fuel rod A.

Table 2 summarizes oxide layer thicknesses and chemical interaction layer thickness for the intact fuel rods A and B and the leak fuel rods C and D. Based on the optical and scanning electron micrographs shown in Figs. 2, 4 and 7–9, it can be said that, for the intact rods, one chemical interaction layer at the pellet–clad interface will form apparently, while, for the leak fuel rods, two chemical interaction layers will form apparently. In order to determine the phases of chemical interaction layers formed at the interfaces for the intact and leak fuel rods, the U–Zr–O ternary phase diagram [11,12] is used, as shown in Fig. 10. It should be noted that the U–Zr–O ternary phase diagram showing phases at 1000 °C was used, extrapolating to the normal reactor operation temperature ranges of between 400–500 °C. It should be noted that U–Zr–O ternary phase diagrams at temperatures of between 400–500 °C are needed to predict phases of chemical interaction layers at such normal operation temperature. However, U–Zr–O ternary phase diagrams below 1000 °C are not available. In this paper, therefore, the U–Zr–O ternary phase diagram at 1000 °C is employed as the first trial to evaluate how it would predict the interaction layers formed at such operating temperatures using diffusion paths, considering that all the phases existing at 1000 °C are solid just like those at temperatures below 1000 °C and the phases at 1000 °C are probably the same as those at temperatures below for 1000 °C even though detailed phase compositions at 1000 °C are quite different from those at temperatures below 1000 °C. The waterside oxide thickness of the Zircaloy cladding increases with the increase of burnup, resulting in the increase of oxygen concentration in the cladding metal portion. The pellet–cladding hard contact is necessary to produce the chemical interaction layers at the pellet–cladding interface. The hard contact may appear at mid-axial positions except the upper and lower axial locations when the rod average burnup increases to 25,000–35,000 MWD/MTU, depending on cladding materials and rod power histories. However, since the fuel rods considered in this study have the burnup of between 35,000 and 53,000 MWD/MTU, one can say that the hard contact definitely occurred at mid-axial positions. In general, oxides are formed at the cladding outer surface and subsequently oxygen diffuses into the remaining Zr metal region, resulting in the increase of oxygen concentration in the metal and subsequently changing pure Zr into α-Zr(O). In detail, Figs. 3 and 5 show that the oxygen content of the pure Zr increases to initially form the oxygen-deficient α-Zr(O)$_I$ phase and subsequently increases up to 30 mol to form oxygen-saturated α-Zr(O)$_{II}$ in the

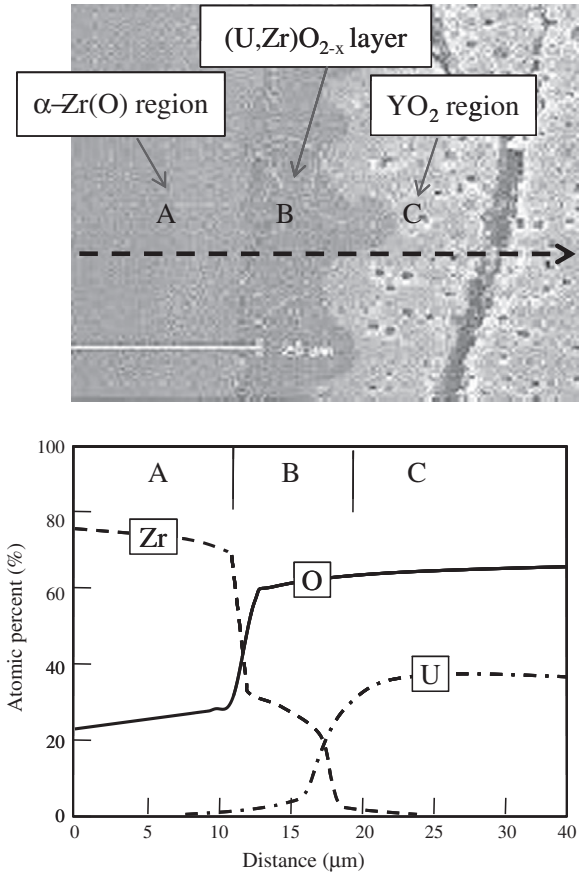

Fig. 5. Concentration distributions of U, Zr and O across the cladding and the pellet.

cladding outer surface area. The oxygen-saturated α-Zr(O)$_{II}$ phase can absorb more oxygen and then it is transformed into the ZrO_2 phase, while most of α-Zr(O) in the cladding may exist as oxygen-deficient phase during the fuel lifetime if there is no the hard contact between cladding inner surface and pellet. On the other hand, with the hard contact forming at the interface of the intact fuel rods A and B, the oxygen-deficient α-Zr(O)$_I$ phase at the cladding inner surface will react with UO_2 pellet since α-Zr(O) is thermodynamically unstable with respect to UO_2. For the intact fuel rods, it should be noted that the UO_2 pellet supplies oxygen to the α-Zr(O)$_I$ phase contacting the UO_2 pellet. According to the diffusion paths given in the U–Zr–O phase diagram shown in Fig. 10, the oxygen-deficient α-Zr(O)$_I$ phase at the interface may turn into oxygen-saturated α-Zr(O)$_{II}$ by absorbing oxygen from the UO_2 pellet side by the diffusion path a–b, leaving UO_2 as UO_{2-x} at the interface by the diffusion path c–d. However, it is noted that the UO_{2-x} phase exists as [UO_2 + U] phases at the reactor operating temperature range since it is unstable below about 1000 °C and transformed into [UO_2 + U] phases. In parallel, Zr and U may interdiffuse into UO_{2-x} and α-Zr(O)$_{II}$, respectively, finally resulting in cubic $(U,Zr)O_{2-x}$ and α-Zr(O)$_{II}$ phases at the interface by the diffusion path b–c. For the intact fuel rods A and B, therefore, the newly formed chemical interaction layers at the pellet–cladding interface are oxygen-saturated α-Zr(O)$_{II}$ and $(U,Zr)O_{2-x}$ that may be seen in the Fig. 4. The composition changes in U, Zr and O elements are shown in Fig. 5. Similarly the UO_2 pellet region adjacent to the $(U,Zr)O_{2-x}$ interaction layer turns into UO_{2-x} which actually exists as [UO_2 + U] phases in the low temperature range, as explained above. However, it should be noted that the optical micrographs of the intact fuel rods show a grey $(U,Zr)O_{2-x}$ layer only, as seen in Figs. 2 and 7. From Figs. 4 and 5, it can be seen that the Zr composition drops sharply when moving into the pellet side, while the U composition drops sharply when moving into the cladding side but the oxygen content is nearly constant in the $(U,Zr)O_{2-x}$ layer. From the cladding outside, therefore, the sequence of various phases across the cladding and pellet for the intact rods may be written as:

$$[ZrO_2] \rightarrow [\text{oxygen-deficient } \alpha\text{-Zr(O)}_I] \rightarrow [\text{oxygen-saturated } \alpha\text{-Zr(O)}_{II}] \rightarrow [\text{cubic } (U,Zr)O_{2-x}] \rightarrow [UO_2 + U] \rightarrow [UO_2].$$

These interaction layers are a little different from those obtained from other out-of-pile experiments with pure Zry–UO_2 specimens performed at the temperatures of between 1000 and 1700 °C [7]. According to [7], the sequence of various phases across the cladding and pellet is summarized as:

$$\text{Pure Zry} \rightarrow \alpha\text{-Zr(O)} \rightarrow [U,Zr] \rightarrow [\alpha\text{-Zr(O)} + (U,Zr)] \rightarrow [UO_2]$$

This difference in interaction phases may be explained by the fact that the fuel rods examined in this study have much higher oxygen content in the cladding metal region prior to the hard

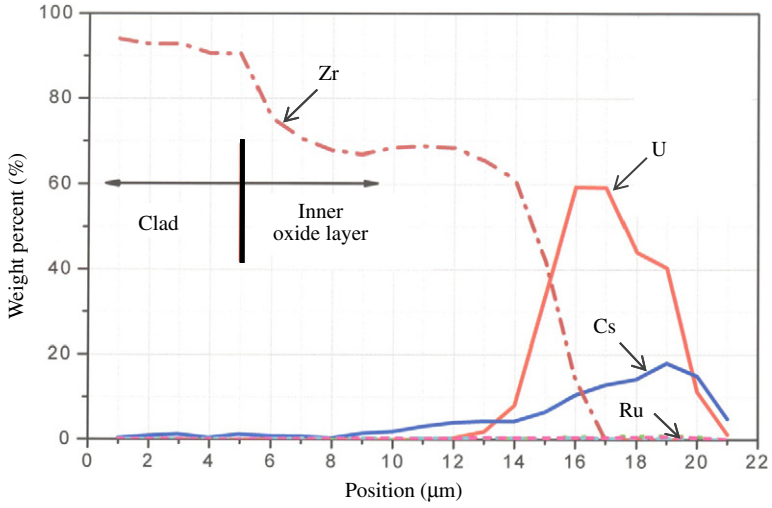

Fig. 6. Concentration distributions of various chemical elements across the cladding and the pellet.

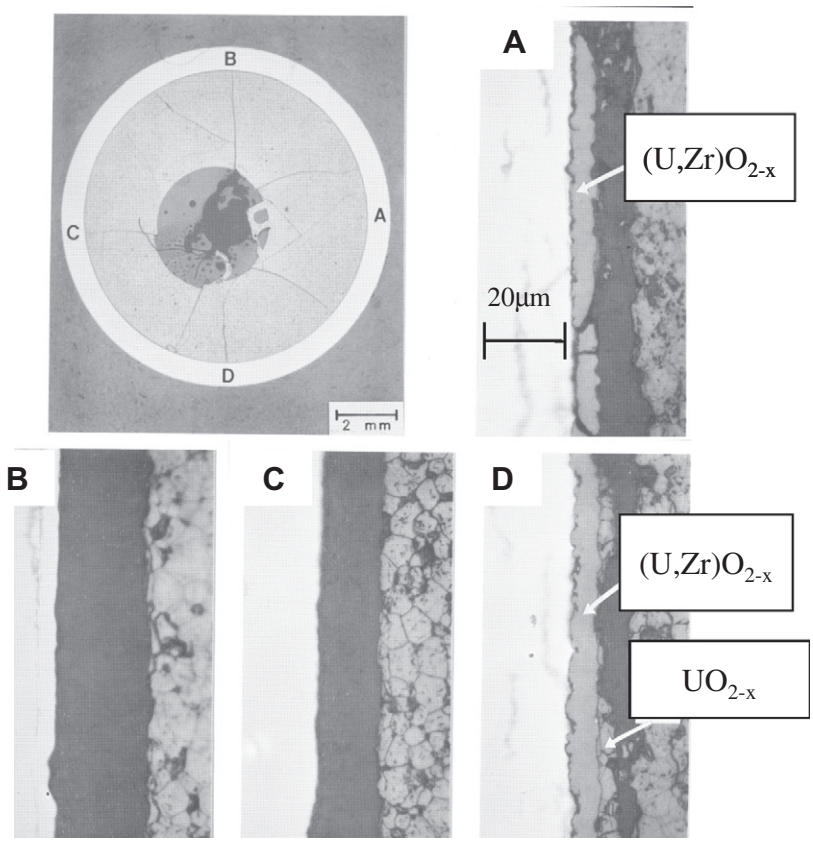

Fig. 7. Optical micrographs of intact fuel rod B.

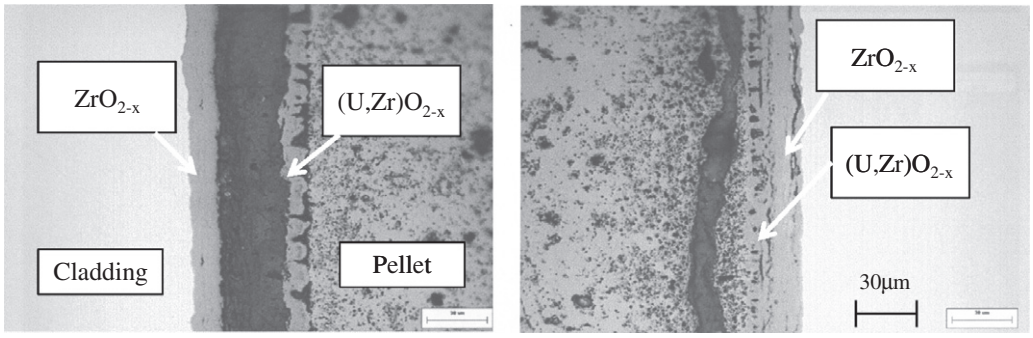

Fig. 8. Optical micrographs of leak fuel rod C.

contact at the interface and also have lower reaction temperatures than the pure Zry–UO_2 specimens used in [7]. The UO_2 phase in [7] should be interpreted as [UO_2 + U] and UO_2 phases. The phases given in [7] can be predicted by the diffusion path a–bb–d–e of the U–Zr–O phase diagram shown in Fig. 10, considering the lower oxygen content in the Zr metal. The diffusion path a–bb predicts α-Zr(O) and (U,Zr) phases at the α-Zr(O)–(U,Zr) interface, the diffusion path bb–d predicts (U,Zr), α-Zr(O) and UO_{2-x} phases at the [α-Zr(O) + (U,Zr)]–UO_2 interface, and the diffusion path d–e predicts UO_{2-x} and UO_2 phases.

More oxygen is supplied to the pellet–clad gap for the leak fuel rods C and D than the intact rods A and B because the leak rods have an additional oxygen source from steam coming into the pellet–clad gap. For the leak fuel rods, therefore, one has to determine onset time (or burnup) for both the hard contact formation and the cladding breach allowing water into the gap. Then, the water in the gap is transformed into steam due to a relatively high temperature in the gap. If the hard contact occurs earlier than the cladding breach, oxygen-saturated α-$Zr(O)_{II}$ and the cubic $(U,Zr)O_{2-x}$ phases will form at the interface before the cladding breach by the diffusion path a–b–c–d–e, as explained for the intact rods. After the cladding breach, further absorption of oxygen in the oxygen-saturated α-$Zr(O)_{II}$ phase contacting the $(U,Zr)O_{2-x}$ phase will be converted into the monoclinic ZrO_{2-x} phase at the α-$Zr(O)_{II}$-$(U,Zr)O_{2-x}$ interface by the diffusion path b–h shown in Fig. 10. When the monoclinic ZrO_{2-x} phase forms between the α-$Zr(O)_{II}$ and cubic $(U,Zr)O_{2-x}$ phases, the chemical interaction between monoclinic ZrO_{2-x} and cubic $(U,Zr)O_{2-x}$ phases may proceed to produce Zr-rich monoclinic $(U,Zr)O_{2-x}$ phase at the ZrO_{2-x}–cubic $(U,Zr)O_{2-x}$ interface, according to the diffusion path f–g–h shown in Fig. 10.

If the cladding breach occurs earlier than the hard contact, however, the monoclinic ZrO_2 phase will form at the cladding inner surface prior to the pellet–clad hard contact, as indicated by the diffusion path b–h–i shown in Fig. 10. When the growing ZrO_2

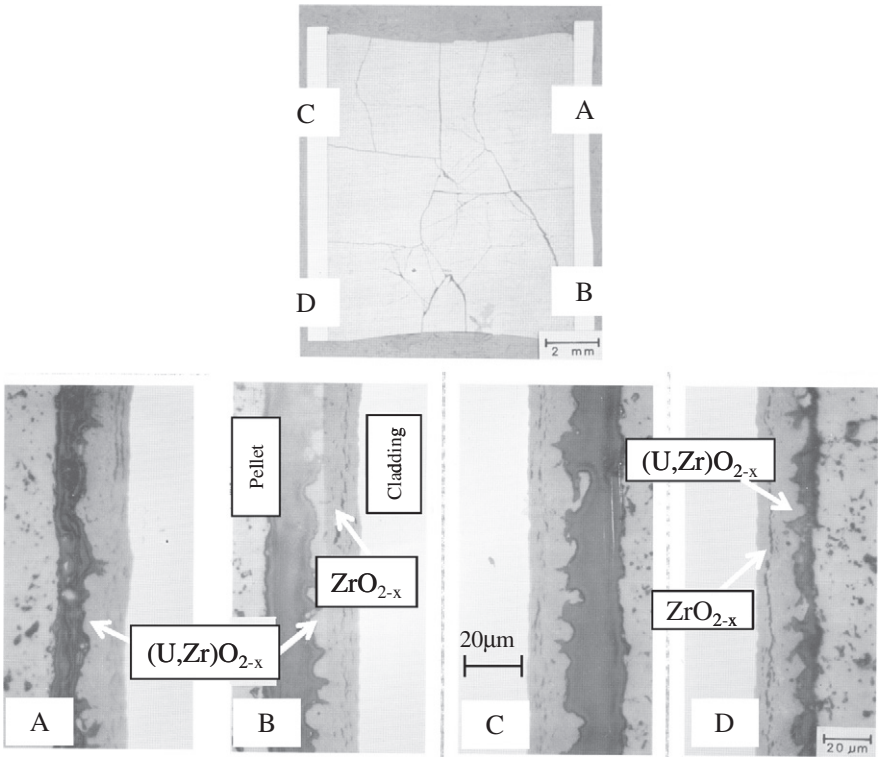

Fig. 9. Optical micrographs of leak fuel rod D.

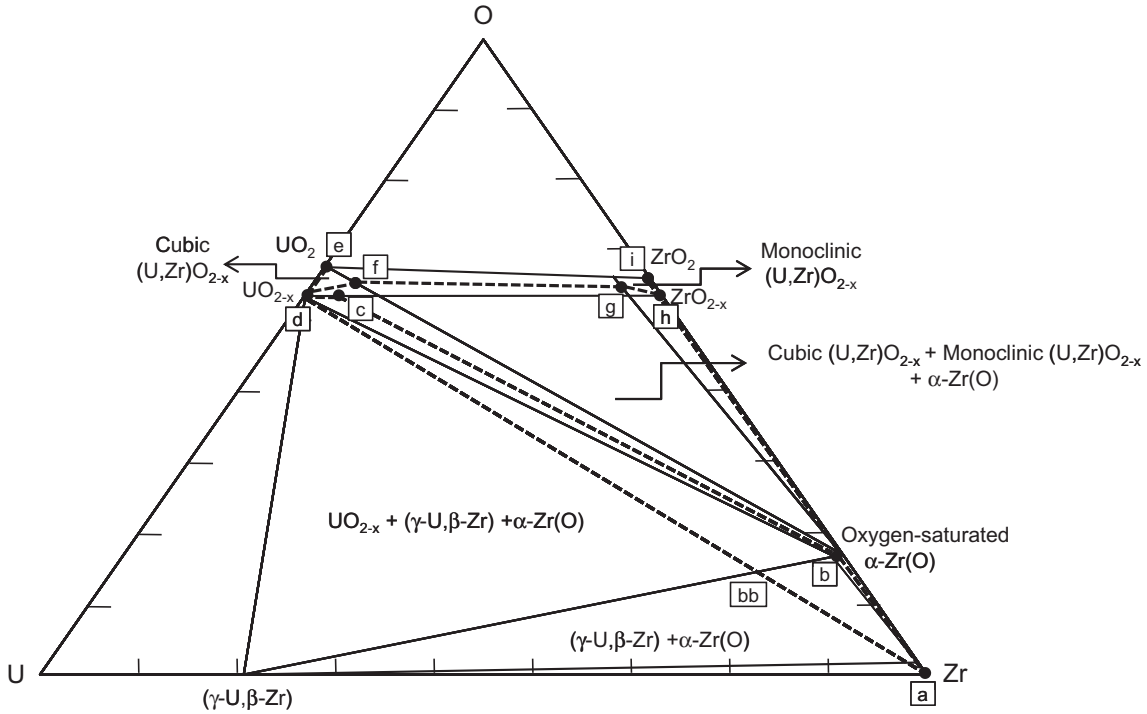

Fig. 10. Diffusion paths in the U–Zr–O ternary phase diagram at 1000 °C.

phase with time finally contacts the UO_2 pellet, the ZrO_2–UO_2 contacting phases will react to produce ZrO_{2-x}, Zr-rich monoclinic $(U,Zr)O_{2-x}$, U-rich cubic $(U,Zr)O_{2-x}$ and UO_{2-x} phases at the ZrO_2–UO_2 interface, as indicated by the diffusion path i–h–g–f–d–e shown in Fig. 10.

According to Nogita and Une [10], however, the monoclinic $(U,Zr)O_{2-x}$ phase was not observed at the pellet–cladding interface in high burnup BWR fuels. They explained that the monoclinic phase transformed into cubic phase possibly due to the stress-induced phase transformation, formation of stabilized zirconia and fission-induced phase transformation, even though the U–Zr–O phase diagram predicts the monoclinic phase at the pellet–cladding interface. In this study, detailed crystal structure analyses were not performed to confirm the transformation of the monoclinic $(U,Zr)O_{2-x}$ phase into the cubic $(U,Zr)O_{2-x}$ phase observed in [10]. Based on the interaction layer investigation performed in

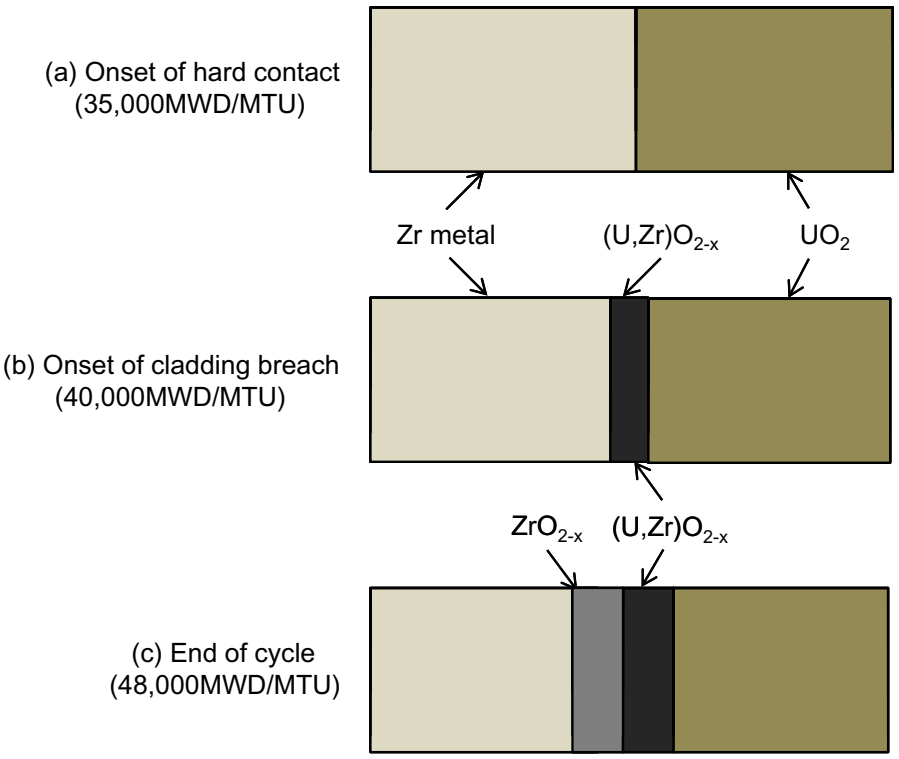

Fig. 11. Schematic diagrams for chemical interaction layers with operation time (leak fuel rod C).

this study, however, it can be said that the U–Zr–O phase diagram at 1000 °C can be used with some confidence in predicting various interaction layers between the cladding/pellet interface, even though the transformation of the monoclinic phase into the cubic phase cannot be predicted.

Using the rod power versus reactor coolant activity analysis, it was found that the leak fuel rod C with the discharge rod burnup of 48,000 MWD/MTU was breached at the rod burnup of about 40,000 MWD/MTU, while the leak fuel rod D with the discharge rod burnup of 35,000 MWD/MTU was breached at the rod burnup of about 22,000 MWD/MTU. In addition, the pellet–clad hard contact may initiate at 35,000 and 25,000 MWD/MTU for the leak rods C and D, respectively, based on the rod power histories and the irradiation-induced fuel materials behaviors. Therefore, it can be said that for the leak rod C, the hard contact might occur before the cladding breach, whereas for the leak rod D, the cladding breach might occur before the hard contact. The schematic diagrams for the leak rods, C and D, are shown in Figs. 11 and 12, indicating various interaction layers formed at the pellet–cladding interface as a function of burnup, as explained above. Even though the order of the hard contact and the cladding breach are opposite for the two leak fuel rods, however, final interaction layers at the cladding–pellet interface are the same but their microstructures are a little different. The phases across the cladding and pellet for the leak rods may be summarized as:

$$[ZrO_2] \rightarrow [\text{oxygen-deficient } \alpha\text{-Zr(O)}] \rightarrow [\text{oxygen-saturated } \alpha\text{-Zr(O)}] \rightarrow [ZrO_{2-x}] \rightarrow [\text{Zr-rich monoclinic } (U,Zr)O_{2-x}] \rightarrow [\text{U-rich cubic } (U,Zr)O_{2-x}] \rightarrow [UO_2 + U] \rightarrow [UO_2].$$

It should be noted that the optical micrographs shows only two interaction layers, ZrO_{2-x} and cubic $(U,Zr)O_{2-x}$, at the pellet–cladding interface since the Zr-rich monoclinic $(U,Zr)O_{2-x}$ and U-rich cubic $(U,Zr)O_{2-x}$ cannot be distinguished by the optical microscopy.

From Table 2, the $(U,Zr)O_{2-x}$ layer thicknesses for the intact rods A and B are 12 and 9 μm, respectively. The ZrO_2 layer thicknesses for the leak rods C and D are 15 μm, while the $(U,Zr)O_{2-x}$ layer thicknesses for them are 12 and 6 μm, respectively. Assuming the reactor operating conditions of the fuel rods A an C for the three-loop plant and their fuel rod power histories, the onset time of the pellet–cladding hard contact for the fuel rod is estimated to be 850 days from the beginning of life, while that of the cladding breach 1100 days from the beginning of life, based on the coolant activity data. In addition, assuming the reactor operating conditions of the fuel rods B and D for the two-loop plant and their fuel rod power histories, the onset time of the pellet–cladding hard contact for the fuel rod is estimated to be 450 days from the beginning of life, while that of the cladding breach 430 days from the beginning of life, based on the coolant activity data. The total residence time of the fuel rods A and C is 1266 days, whereas that of the fuel rods B and D is 710 days. Considering the total residence times, the cladding breach times and the pellet–clad hard contact times, the interaction times for $(U,Zr)O_{2-x}$ and ZrO_{2-x} were calculated, as given in Table 2. Then, the interaction layer growth rates for the fuel rods A, B, C and D are given in Table 2, which were calculated with the use of the interaction layer thicknesses and the relevant interaction times. With the use of the fuel performance code [14], the pellet–cladding interface temperature is calculated to be 400 °C and 380 °C, respectively, for the two-loop and three-loop fuel rods. Using these temperatures and the interaction times given in Table 2, the built-in ZrO_2 oxidation models of the fuel rod design code [15] predicted that the ZrO_2 layer thicknesses are 12 and 13 μm for the leak fuel rods C and D, respectively. These predicted values are in fairly good agreement with the aforementioned measured ones. The comparison of the $(U,Zr)O_{2-x}$ growth rate for the intact rods and the ZrO_2 growth rate for the leak rods given in Table 2 indicates that the $(U,Zr)O_{2-x}$ layer grows at nearly the same rate as the ZrO_2 layer. However, the $(U,Zr)O_{2-x}$ layer growth rate for the leak fuel rod D is much smaller than that for the leak fuel rod C. This

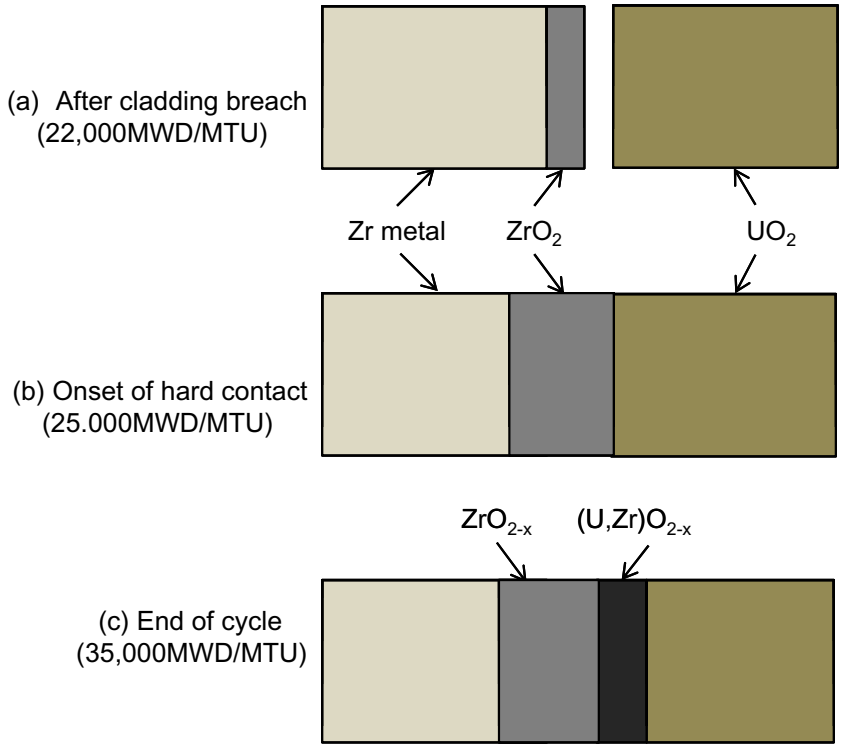

Fig. 12. Schematic diagrams for chemical interaction layers with operation time (leak fuel rod D).

may indicate that the already-formed ZrO_2 layer on the cladding inner surface for the fuel rod D will retard the $(U,Zr)O_{2-x}$ layer growth after the pellet–cladding hard contact since the oxygen potential difference between $(U,Zr)O_{2-x}$ and ZrO_{2-x} is much smaller than that between $(U,Zr)O_{2-x}$ and α-Zr(O). In this paper, the kinetics of the interaction layer growths and rate controlling diffusion mechanisms in each interaction layer are not investigated since the necessary kinetic and thermodynamic data are not all available at the normal reactor operating temperatures. However, it should be noted that Olander [16] predicted interaction layer growth rates formed at the UO_2 pellet–Zircaloy-4 cladding at a relatively high temperature of 1500 °C with a model that accounts for the formation and growth of interaction layers. According to [16], the kinetics of the process is governed by diffusion of oxygen and uranium in the interaction layers with chemical equilibrium at each interface.

4. Conclusions

The Zry-4/UO_2 chemical interactions for the intact and leak PWR fuel rods were investigated and the results can be summarized as follows:

1. The $(U,Zr)O_{2-x}$ interaction layer at the pellet–cladding interface for the intact fuel rods was observed with the help of an optical microscope and a scanning electron microscope. However, the actual chemical interaction layers at the interface might be composed of oxygen-saturated α-$Zr(O)_{II}$, cubic $(U,Zr)O_{2-x}$ and $[UO_2 + U]$ phases, based on the diffusion paths in the Zr–UO_2 binary phase diagram and the U–Zr–O ternary one. The composition variations of U, Zr and O generated by EPMA may confirm the $(U,Zr)O_{2-x}$ interaction layer.
2. The ZrO_2 and $(U,Zr)O_{2-x}$ interaction layers at the pellet–cladding interface for the leak fuel rods were observed with the help of an optical microscope. However, the actual chemical interaction layers at the interface might be composed of oxygen-saturated α-$Zr(O)_{II}$, ZrO_{2-x}, monoclinic $(U,Zr)O_{2-x}$, cubic $(U,Zr)O_{2-x}$ and $[UO_2 + U]$, based on the diffusion paths in the U–Zr–O ternary phase diagram.
3. The growth rates of the $(U,Zr)O_{2-x}$ and ZrO_2 interaction layers were calculated, considering the parameters such as the measured layer thicknesses, reaction temperatures at the interface, the onset times of the cladding breach and the hard contact appearance. They are fairly in good agreement with the growth rates predicted by the ZrO_2 oxidation kinetics.

Acknowledgements

This research was supported by Basic Atomic Energy Research Institute Program through the National Research Foundation of Korea (NRF) funded by the Ministry of Education, Science and Technology (No. 2009-0075907).

References

[1] K. Kim, D.R. Olander, J. Nucl. Mater. 154 (1988) 85–101.
[2] K. Kim, D.R. Olander, J. Nucl. Mater. 154 (1988) 102–115.
[3] P. Hofmann, Dissolution of solid UO_2 fuel by molten zircaloy-4 Cladding, in: Severe Fuel Damage Program Review Meeting, Oak Ridge, TN, 1986.
[4] H.E. Rosinger, K. Demoline, R.K. Rondeau, Dissolution of UO_2 by molten zircaloy-4 cladding, in: Fifth International Conference on Thermal Nuclear Reactor Safety, Karlsruhe, Germany, 1984.
[5] P.J. Hayward, I.M. George, J. Nucl. Mater. 232(1996)1–12.
[6] P.J. Hayward, I.M. George, J. Nucl. Mater. 232(1996)13–22.
[7] P. Hofmann, H.J. Neutzel, Experimental and theoretical results of cladding oxidation under severe fuel damage conditions, in: Seventh International Conference on Zirconium in the Nuclear Industry, Strasbourg, France, 1985.
[8] S. Berghe, A. Leenaers, B. Sannen, M. Verwerft, Observation of a pellet–cladding bonding layer in high-power fuel, in: Seminar Proceedings on Pellet-to-Clad Interaction in Water Reactor Fuels, Aix-en-Provence, France, 2004.
[9] K. Nogita, K. Une, Y. Korei, Instrum. Method. Phys. Res. Sect. B 116 (1996) 521–526.
[10] K. Nogita, K. Une, J. Nucl. Sci. Technol. 34 (1997) 679–686.

[11] C. Politis, Investigation of the Ternary Uranium–Zirconium–Oxygen System, KfK2167, 1975.
[12] A. Skokan, High temperature phase relations in the U–Zr–O system, in: Fifth International Meeting on Thermal Nuclear Reactor Safety, Karlsruhe, Germany, 1984.
[13] V.F. Urbanic, J. Nucl. Mater. 75 (1978) 251–261.
[14] R. Eberle, The KWU Fuel Rod Computer Code CARO (Version D5), KWU TR B111/82/e117a.
[15] ABB/CE, Fuel Evaluation Model, CENPD-139-P-A, July 1974.
[16] D.R. Olander, J. Nucl. Mater. 115 (1983) 271–285.